CARBON 57 (2013) 507–514

Available at www.sciencedirect.com

SciVerse ScienceDirect

journal homepage: www.elsevier.com/locate/carbon

Stable p- and n-type doping of few-layer graphene/graphite

Xiuqing Meng [a], Sefaattin Tongay [b], Jun Kang [c], Zhanghui Chen [c], Fengmin Wu [a], Shu-Shen Li [c], Jian-Bai Xia [c], Jingbo Li [a,c,*], Junqiao Wu [b,*]

[a] Research Center for Light Emitting Diodes (LED), Zhejiang Normal University, Jinhua 321004, China
[b] Department of Materials Science and Engineering, University of California, Berkeley, CA 94720, USA
[c] State Key Laboratory of Superlattices and Microstructures, Institute of Semiconductors, Chinese Academy of Sciences, Beijing 100083, China

ARTICLE INFO

Article history:
Received 17 August 2012
Accepted 10 February 2013
Available online 19 February 2013

ABSTRACT

ZnMg and $NbCl_5$ were intercalated in graphite and the presence of such molecules between the graphene sheets results in n- and p-type doping, respectively. The doping effect is confirmed by Hall and Raman measurements and the intercalation process is monitored by scanning tunneling microscopy. After intercalation the carrier concentration increase almost an order of magnitude and reaches values as high as $10^{19}$and 10^{18} cm^{-3} for p- and n-type doping, respectively. For higher intercalation times, the intercalated graphite turns back to be as ordered as pristine one as evidenced by the reduction in the D peak in Raman measurements. Intercalation compounds show remarkable stability allowing us to permanently tune the physical properties of few-layer graphite. Our study has provided a new route to produce stable and functional graphite intercalation compounds and the results can be applied to other graphitic structures such as few-layer graphene on SiC.

1. Introduction

Recently, interest in the synthesis and physical properties of the graphite intercalation compounds (GICs) has been renewed as they not only possess many novel features in structural, electronic, and optical properties [1–11] but also allows one to adjust graphene and few-layer graphene's (FLG) physical properties [8–11]. It is well known that graphite with Bernal stacking (ABAB) has a layered structure with 3.35 Å interlayer distance. This interlayer distance is large enough for certain ions and/or molecules (intercalants) to be intercalated between the layers. During the intercalation process, intercalants interact with the host material and transfer charges (electron or holes) to carbon atoms resulting doping the material. So far, alkali-earth metals (i.e. Li, K, Mg, Ca) and halogens (Cl_2, Br_2, I_2) have been used as donor and acceptor intercalants, respectively and these GICs have been readily employed in electrodes, conductors, superconductors, catalysts, hydrogen storage materials, diodes, batteries, displays, or polarizers [1–5,8–11]. However, most of the GICs are environmentally unstable either due to desorption of the intercalants overtime, or oxidization upon exposure to air [1]. It has been theoretically predicted that some intercalants such as the p-type $NbCl_5$ and n-type ZnMg could be more stable in intercalated graphite [1,12]. Moreover, these intercalants may also have potential applications in a variety of fields combining the advantage of excellent superconductive properties of Nb and the good mechanical and chemical stability of ZnMg alloy, respectively, with the outstanding properties of graphitic materials.

In this paper, we present the first experimental realization of $NbCl_5$ and ZnMg intercalated graphite by two-zone vapor transport method. We find that $NbCl_5$ and ZnMg intercalation in graphite allow us to achieve p- and n-type doping, respectively. We confirm the doping effect by scanning tunneling microscopy (STM), Raman spectroscopy, Hall measurements,

* *Corresponding authors:* Fax: +86-579-82297913.
E-mail address: jbli@semi.ac.cn (J. Li).
0008-6223/$ - see front matter
http://dx.doi.org/10.1016/j.carbon.2013.02.028

and density functional theory (DFT) calculations. At the initial stages of the intercalation, dopants typically increase the disorder in graphite. The disorder density decreases for increasing intercalation, implying quasi-structural ordering in the intercalated compound. Results reported here not only allow us to tune the Fermi level and carrier density in the bulk limit but also possibly in few-layer graphite grown on SiC where the individual layers behave as graphene sheets.

2. Experimental and theoretical details

2.1. Sample preparation and characterization

Graphite flakes are obtained by micro-mechanical cleavage of natural graphite (NT-MDT Co, Russia) onto SiO_2 (300 nm)/Si substrates. In this work, n- and p-type doping of the graphite have been achieved by intercalating $NbCl_5$ and ZnMg alloy using two-zone vapor transport process. (1) For $NbCl_5$–graphite synthesis, the intercalant (from Aladdin reagent) and the graphite flakes are positioned in different zones in a glass ampoule and then the ampoule was pumped to 5 mTorr and sealed. Sealed glass ampoule was inserted in a tube furnace and kept at 420 °C for different periods of time depending on the desired amount of intercalation and the temperature difference between the intercalant and graphite flakes was kept at 90 °C during the intercalation. (2) for ZnMg–graphite synthesis, the intercalant and the graphite flakes are sealed in a vacuum sealed quartz tube and kept at 600 °C for various times to monitor progression of the intercalation process. The structural characterization of the samples were performed using X-ray diffraction (XRD) technique using Cu Kα irradiation, the atomic scale structures are examined by STM measurement carried with a applied bias voltage of 50 mV. X-ray photoelectron spectroscopy (XPS) measurements were carried out on VGESCALAB MK II instrument. Raman spectrum was measured using a micro-Raman spectrometer with 514 nm laser as excitation source on a different spots and the Hall measurements were carried out by a Ecopia HMS-300 Hall effect measurement system. All the measurements are performed at room temperature in the super-clean room under the same condition after the samples are just taken out from the ampoules and the reproducibility of the results have been tested on different samples as well as different spots on the same sample.

2.2. Density functional theory calculations

To obtain globally optimal structure of metal clusters, we use Gupta potential and Evolutionary Algorithms [13,14] to model clusters. A common growing initialization operator, "cut-and-splice" crossover [15] and triangle mutation [16] are used to search the global structure and then Limited-memory Broyden–Fletcher–Goldfarb–Shanno (L-BFGS) operator [17] is used to locate the current local optima. The two processes are repeated until finding the best structures. Optimized clusters are placed between two layers of graphite, each of which contains 12×12 primitive cell and 288 atoms. The whole system is optimized by Forcite with Universal potential, so as to obtain the optimal doping structures. The optimized doping structures are finally calculated using DFT, in which the total energy and electronic structure calculations are performed using the projector augmented wave (PAW) formalism [18,19] and a plane wave basis set, as implemented in the Vienna ab initio simulation package (VASP) [20,21]. The exchange and correlation potential are treated in the framework of generalized gradient approximation (GGA) of Perdew–Burke–Ernzerbof (PBE) [22]. The wave functions are expanded in plane waves up to a cutoff of 207.5 eV and the convergence precision of the total energy is set to be lower than 1 meV. For the summation of charge densities over a Brillouin zone, a $1 \times 1 \times 1$ Monkhorst–Pack [23] k-point mesh is adopted. Then the Eigen values at high symmetry k-points are calculated using the charge densities, and the band structure is obtained. To simulate $NbCl_5$ intercalated graphite, we construct a 4×4 supercell of two-layer graphite with AA stacking, and the supercell contains one $NbCl_5$ molecule which is intercalated between the two graphite layers. The optimized distance between the two graphene layers is about 9 Å, which is much larger than that in pure graphite due to the intercalation of $NbCl_5$. The Brillouin zone is sampled by a $5 \times 5 \times 1$ Monkhorst–Pack mesh. The structure is relaxed so that the Hellmann–Feynman forces acting on each atom is less than 0.02 eV/Å.

3. Results and discussion

In Fig. 1, we show the STM images of pristine and intercalated graphite samples taken at room temperature in the super-clean room after the samples are just taken out from the ampoules under the same conditions. Before intercalation, clear hexagonally arranged carbon atoms are observed on the pristine graphite samples (Fig. 1a) and three dimensional patterns shown in Fig. 1d indicate that the height of all the carbon atoms are almost in the same horizontal lines. The STM images taken on the intercalated graphite show regions with islands distributed in the images. The observed regions of the islands may originate from locally missing intercalations, most likely in subsurface parts of the sample. However, the observed islands sometimes indicate inhomogeneities in the spatial distribution of the intercalations, rather than representing topographic surface structure only [24]. On the other hand, on intercalated regions where the intercalates are placed just underneath the basal plane of the graphite observed, therefore, STM images in atomic scale could be a method to characterize whether or not intercalation have taken place [25]. From Fig. 1b and c we find that the intercalants are successfully intercalated between the graphene sheets in the form of clusters, the clusters are distributed in the whole observed region. Generally, an STM image reflects not only the geometric structure but also the density of states [26]. The real height of the STM image is analysized. The bright region is found to be higher than the dark region by 0.20–0.30 nm, which is smaller than the apparent height. The sizes of the bright regions typically range from 0.5 to 2 nm wide and about 0.4–0.5 nm deep. The contrast is considered mainly corresponds to the height modulation and the intact top carbon layer is corrugated. In the present study, the bright and the dark regions observed in the STM image are considered to

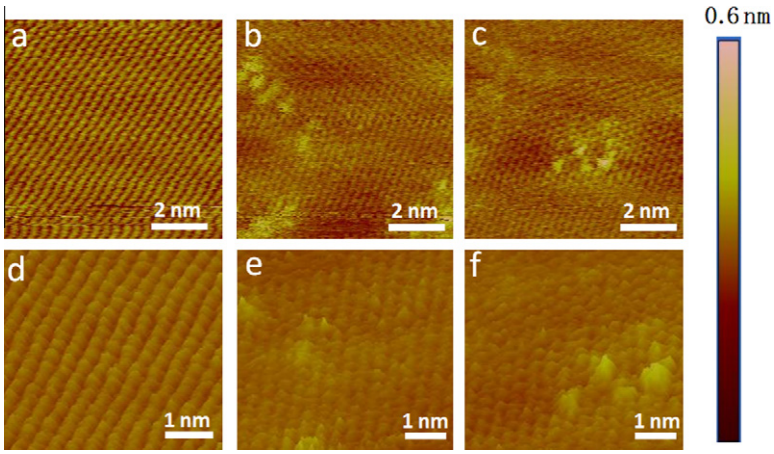

Fig. 1 – STM image of the pristine graphite, $NbCl_5$ intercalated graphite (87 h) and ZnMg intercalated graphite (48 h) (a–c) and their corresponding three dimensional images (d–f). The right scale bar is a color scale bar of figure (a–c). All the images are taken as original and no drift correction is performed.

correspond to the $NbCl_5$ or ZnMg–intercalated regions and the $NbCl_5$ or ZnMg-free domains, respectively. The bright regions in the STM image is also inhomogeneous, showing the overlap of bright regions, caused by the overlapping of nano-valleys in different carbon layers [27].

While the physical process governing the ZnMg intercalation is not very straightforward, intercalation of $NbCl_5$ can be interpreted as follows: as Nb^{5+} and Cl^- are combined by ionic bonds, Nb atoms intercalate between the two graphite layers with Cl atoms occupying preferred sites associated with the graphene lattice [1,28]. Intercalants tend to locally increase the lattice constant (reduce the coupling between the graphene layers), which gives bright domains as seen in the GICs images (Fig. 1b and c). For $NbCl_5$–GICs, the contrast between the light and dark regions is not as evident as for the ZnMg intercalated graphite. The most possible reason is that the atomic radius of ZnMg alloy is slightly larger than that of Nb, leading to larger heaves in ZnMg intercalated regions. The three dimensional image of the GICs shown in Fig. 1e and f indicate that surfaces are not as smooth as the pristine graphite. We further confirm the intercalation of ZnMg and $NbCl_5$ from XPS taken on pristine and interacted graphite. In Fig. 2a–c, we observe that additional peaks appear in the XPS spectrum of graphite after the ZnMg and $NbCl_5$ intercalation. These peaks are located at 198, 209, 48, and 1020 eV and are identified as Cl 2p, Nb 3d, Mg 2p, and Zn 2p accordingly. Such measurements clearly provide a direct evidence of presence of such elements.

We also note that the intercalated samples do not display any staging effect, where the intercalants are arranged in a particular form, as the intercalants are randomly distributed between the graphene layers. We further display the lack of staging in our samples by XRD measurements. Here, the XRD measurements provide valuable information on the staging index of the resulting intercalation compounds by the (00*L*) reflections. For instance, stage-1 (stage-2) compound's unit cell contains one (two) graphene sheet separated by an intercalant layer, and hence the staged GICs' *c*-axis lattice parameter significantly differs from that of graphite. This difference in the *c*-axis parameter results in different (00*L*) diffractograms (reflections) at different 2theta values satisfying Bragg's law [1]. In the absence of staging, the intercalants intercalates between the graphene sheets randomly preventing one to assign single lattice constant value and as a result the *c*-axis lattice parameter is largely un-changed and the XRD (00*L*) reflections remain almost the same. In Fig. 2d, we show the XRD patterns of pristine graphite flakes, $NbCl_5$–GICs for 87 h, and ZnMg–GICs for 48 h with the identity period along the *c*-axis, respectively. Since only sharp (002) diffractive peaks accompanied with weak (004) diffractive peaks are observed in the XRD patterns of the pristine and intercalated samples [29] implying that the staging phenomena are not observed in our samples consistent with the STM measurements. By careful examination, the (00*L*) peaks of the $NbCl_5$ and ZnMg intercalated samples slightly shift to lower angles of about 0.5° and 0.6°, respectively, compared with that of HOPG, we attribute this slight shift to the randomly intercalation.

Previously, it has been shown that the Raman spectrum of the carbonaceous materials is sensitive to the doping, defects, strain, disorder, chemical modifications, edges, and relative orientation of the graphene [30–34]. To this end, Raman spectroscopy provides a detailed understanding of the intercalation and adsorption behavior of $NbCl_5$ and ZnMg. The Raman spectrum of graphene consists of a set of distinct peaks; The D, G and D′ peaks appear around 1350, 1580, and 1610 cm^{-1}, respectively. While G peak corresponds to the E_{2g} phonon (stretching mode) at the Brillouin zone center, the D and D′ peaks originate from defect activated one-phonon double resonance process between K–K′ (intervalley) and K–K (intravalley) symmetry points, respectively [35]. The Raman spectra of the synthesized GICs are shown in Fig. 3a from 1000 to 2000 cm^{-1}. Observed peak at 1581 cm^{-1} corresponds to G mode and the peak position is sensitive to the doping level due to the reduction in the Kohn-anomaly for increasing doping where electron–hole interaction for different energies will be forbidden due to Pauli Exclusion Principle. In other words, when the phonons can excite e–h pairs by electron–phonon interaction, this process results in renormalization of electron and phonon energies which in return gives a correction to the

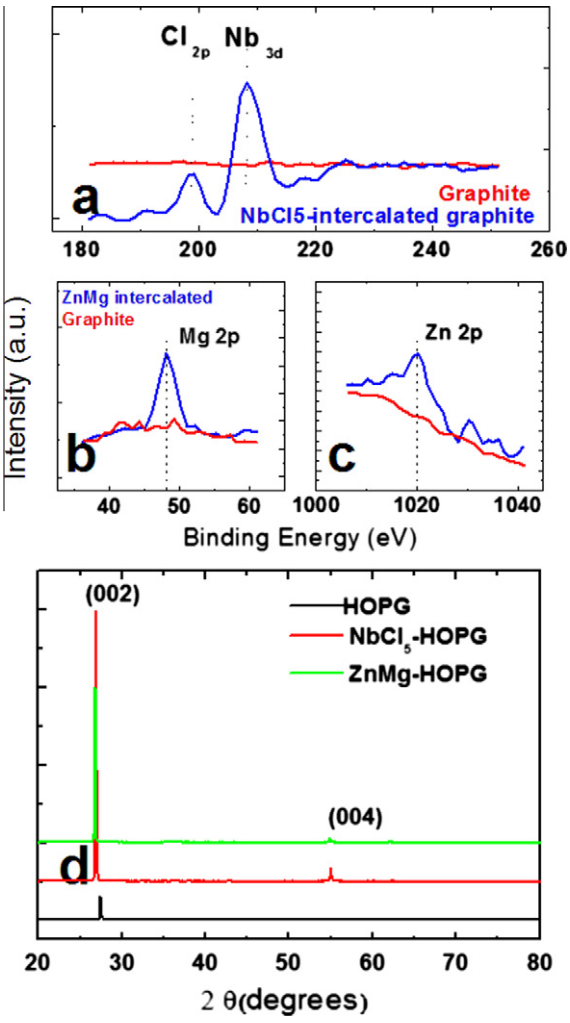

Fig. 2 – XPS spectrum taken on pristine graphite (red line), (a) $NbCl_5$ intercalated graphite for 87 h (blue line) and (b–c) ZnMg intercalated graphite for 48 h (blue line), (d) XRD patterns of the pristine graphite (black), $NbCl_5$ intercalated graphite for 87 h (red) and ZnMg intercalated graphite for 48 h (green), respectively. (For interpretation of the references to colour in this figure legend, the reader is referred to the web version of this article.)

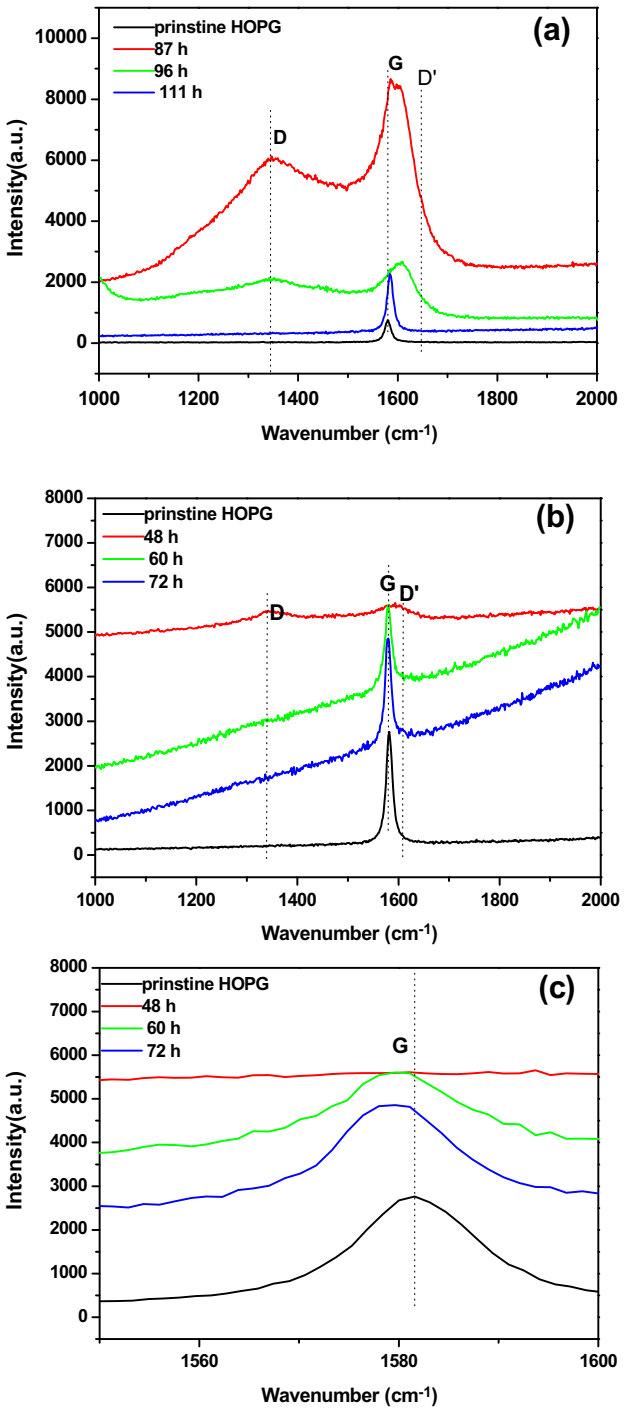

Fig. 3 – Evolution of Raman spectra taken on (a) $NbCl_5$–GICs, (b) ZnMg–GICs at different intercalation times and (c) the magnified part of (b).

peak position of the particular Raman mode. Aforementioned correction to the Raman frequency can be calculated by second-order perturbation theory and this correction term (and hence the actual Raman frequency of the Raman mode) depends on the doping level; under increasing doping, the electron–hole interaction for different energies will be forbidden. As a result, phonons cannot excite e–h pairs by the electron–phonon interaction as easy as in undoped graphene, reducing the correction term to the Raman peak. Such changes, reflects itself as a shift in the peak position [36]. Accordingly, in Fig. 3, we notice that the G peak is blue-shifted by 7 and 9 cm^{-1} for $NbCl_5$–GICs and ZnMg–GICs, respectively. Such change in the G peak position implies that both the $NbCl_5$ and ZnMg molecules are successfully doping the graphite. Moreover, observed G peak shift for $NbCl_5$–GICs is slightly smaller than that of ZnMg–GICs. This slight change might be associated with the different charge transfer ratios for $NbCl_5$ and ZnMg.

After discussing effect of doping on the G peak position, next we focus on the degree of disorder induced during the intercalation. Since the D and D′ peaks are disorder activated, these peaks allow us to identify disorder in the sp^2 bonded carbon structures. Here, we first note that after $NbCl_5$ and ZnMg intercalation, the D peak becomes apparent at around

1350 cm^{-1} implying that the initial stages of intercalation induces disorder in the system. Since the D peak is comparable to the G peak intensity, the D′ peak located at 1610 cm^{-1} also becomes observable and broadens the G peak. At this stage of intercalation, disorder is mostly associated with the sp^2 to sp^3 hybridization transformation where the intercalants are chemisorbed on the graphene sheets. The intensity of the D peak gradually decreases for increasing intercalation times till it completely disappears when the intercalating time reaches 111 h for $NbCl_5$ and 72 h for ZnMg alloy [1–3,28]. Observed reduction in the D and D′ peak intensity might be related with either staging phenomena or partial structural ordering. We eliminate the possibility of staging, since the XRD data taken on the intercalated samples does not show additional XRD peaks. However, the latter effect, partial structural ordering, has been reported before in environmentally unstable Br intercalated graphite where the electron mobility improved after some intercalation threshold time [9] with increasing structural ordering. Similarly, decrease in D peak Raman intensity with increasing intercalation time might be associated with increased (a) dopant uniformity, (b) ordering, and (c) interaction between the intercalants reducing the intercalant–graphite interaction. Regardless from the physical mechanism, reduction in the D peak intensity is advantageous as typically doping in graphene and graphite induces disorder [34] causing electron mobility to decrease.

Hall measurement is a direct method to characterize the electronic properties of the samples. Table 1 shows the Hall measurement results for pristine graphite, $NbCl_5$–GICs for 87 h and ZnMg–GICs for 48 h, respectively. Pristine graphite possesses n-type behavior with a carrier concentration of about 10^{17} cm^{-3} and mobility of 180 cm/V s. When $NbCl_5$ is intercalated, the $NbCl_5$–GICs change to p-type with carrier concentration increased to the level of 10^{19} cm^{-3} although the mobility decreases to about 85 cm/V s. On the other hand, when ZnMg is intercalated, the ZnMg–GICs retain n-type with the carrier concentration and mobility of 1.6×10^{18} cm^{-3} and 138 cm/V s, respectively. The above measurements confirm the effects of intercalation in graphite with $NbCl_5$ as hole dopant and ZnMg as electron dopant, respectively. Moreover, we note that measured Raman peak positions and Hall carriers do not show significant variation over long periods of time, implying that the samples are environmentally stable.

Lastly, we present DFT calculations performed on the $NbCl_5$–GICs and ZnMg–GICs samples. Since the ZnMg powder is in an alloy form, intercalation of ZnMg may result in Mg and Zn clusters and/or Zn_xMg_y binary compound between the graphene layers. To have an idea about the energetic possibility of the ZnMg metal clusters, the binding energy E_b for each metal atom is calculated by:

$$E_b = (E - E_g - nE_{atom})/n$$

Table 1 – Hall measurements of carrier concentrations and mobilities of the non-intercalated graphite, $NbCl_5$ intercalated graphite for 87 h and ZnMg intercalated graphite for 48 h, repectively.

	Carrier concentration (cm^{-3})	Mobility (cm^2/V s)	Conduction type
Graphite	9.8×10^{17}	180	n
$NbCl_5$–graphite	1.16×10^{19}	85	p
ZnMg–graphite	1.6×10^{18}	138	n

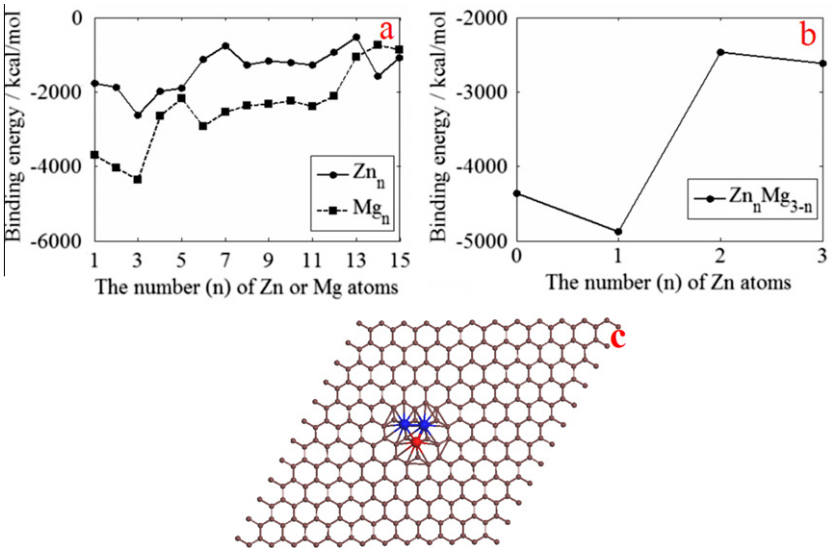

Fig. 4 – Binding energy versus number of (a) Zn (circles), Mg (squares), and (b) ZnMg alloy. (c) Fully relaxed structure of the $ZnMg_2$ cluster between graphene layers.

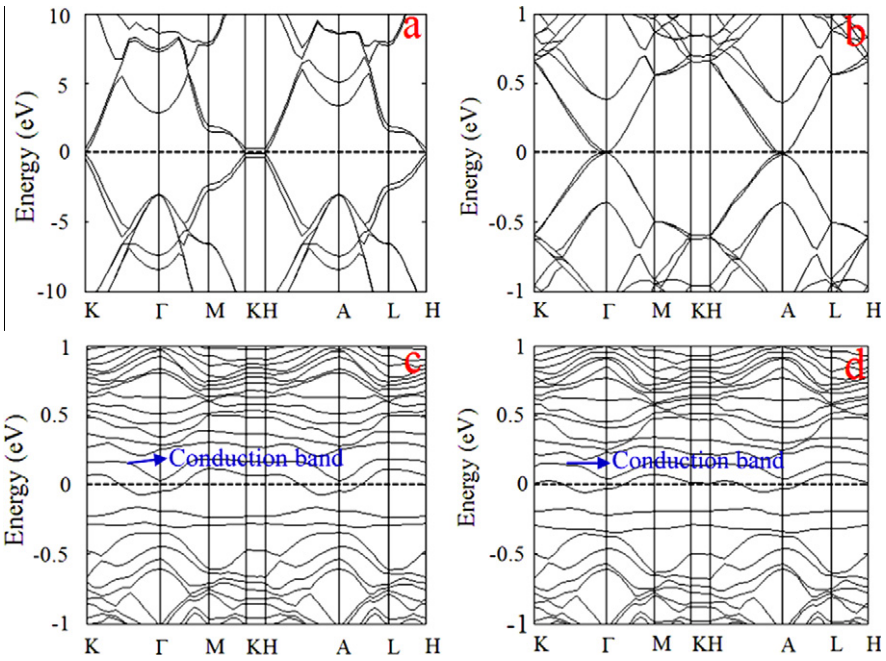

Fig. 5 – The band structure for the system of (a) two layers of graphite (1 × 1 supercell), (b) two layers of graphite (12 × 12 supercell), (c) $ZnMg_2$ and (d) Zn_2Mg within two layers of graphite (12 × 12 supercell). The dotted red line indicates the Fermi level (0 eV). (For interpretation of the references to colour in this figure legend, the reader is referred to the web version of this article.)

where E is the energy of the system containing graphite and metal clusters; E_g is the energy of the graphite system; E_{atom} is the energy of the isolated Zn or Mg atoms.

Fig. 4a shows change in binding energy with respect to the number of Zn or Mg atoms. As shown in Fig. 4a, the binding energy for Zn_3 and Mg_3 is the smallest and thus they are the most stable. However, another possibility is the intercalation of binary compound between the layers. Fig. 4b shows the binding energy of the binary alloy cluster Zn_nMg_{3-n}. We find that the $ZnMg_2$ has the lowest energy and more stable comparing to the other single atom clusters, implying that mostly $ZnMg_2$ cluster is intercalating between the layers while other quasi-stable clusters, i.e. Zn_3 and Mg_3, might be in minority. In Fig. 4c, we show the optimized structure of the $ZnMg_2$ between two graphene sheets. Intercalation of $ZnMg_2$ results in charge transfer (the doping effect) and also chemical interaction. As a result of this interaction, graphene sheet starts bowing around the metal clusters in accord with the STM experiments. Since the ZnMg clusters are more favorable comparing to the elemental clusters, we adopt $ZnMg_2$ and Zn_2Mg as the representative to study the electronic properties of the ZnMg–GICs. Fig. 5 shows band structures calculations for pristine graphite as well as intercalation compounds. As seen in Fig. 5a and b, the conduction

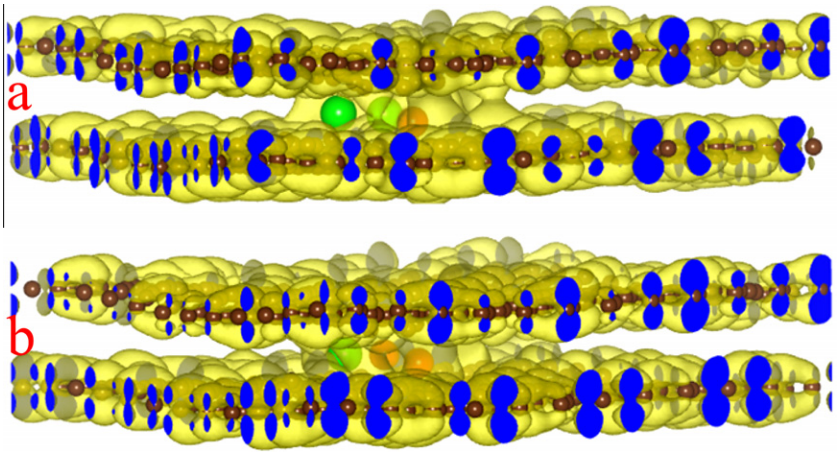

Fig. 6 – The charge density of the conduction band minimum for (a) $ZnMg_2$ and (b) Zn_2Mg within two layers of graphite (12 × 12 supercell). Zn and Mg atoms are indicated by red and green color, respectively. (For interpretation of the references to colour in this figure legend, the reader is referred to the web version of this article.)

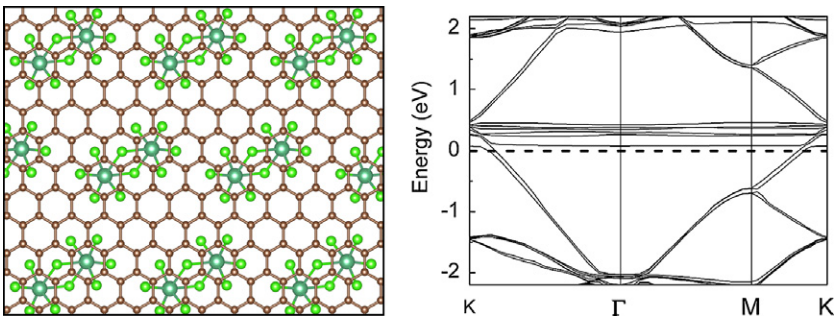

Fig. 7 – (Left) Structure of the model used to simulate $NbCl_5$ intercalated graphite. (Right) Band structure of $NbCl_5$ intercalated graphite. The dash line indicates the Fermi level.

and valance band touches each other at K point for 1×1 supercell while at Γ point for 12×12 supercell. This is due to K and K′ points for the 12×12 supercell of graphite are folded into the Γ point [37]. Therefore, the touching point of the conduction and valance bands for the 12×12 supercell of graphite will be moved to Γ from K point. After the intercalation, we note that the Fermi level enters into the conduction band for $ZnMg_2$ and Zn_2Mg consistent with the n-type doping effect as illustrated before. In addition, the system of the two layers of graphite has a band overlap about 5.5 meV in Γ point (Fig. 5b) [38]. Compared with it, the band of the doping systems is opened and the gap is about 76.4 and 70.8 meV for $ZnMg_2$ and Zn_2Mg at the Γ point. This can be attributed to the re-arranged C atoms near metal clusters. Fig. 6 further shows the charge density of the conduction band minimum for the two systems. It can be found that the charge density is mainly contributed by the orbitals of C atoms, indicating that Zn and Mg atoms open the band gap of the graphite and shift up its conduction band. Similar calculations performed on $NbCl_5$ intercalation also yield similar effects discussed above (see Section 2). The calculated band structure is shown in Fig. 7. It can be clearly seen that the Fermi level enters the π band of graphite, indicating a p-type doping effect of $NbCl_5$ intercalation, which is consistent with the experiment observations.

4. Summary

We have presented the first experimental realization of $NbCl_5$ and ZnMg intercalated graphite by two-zone vapor transport method. We find that $NbCl_5$ and ZnMg intercalation in graphite allow us to achieve p- and n-type doping, respectively. We confirm the doping effect by scanning tunneling microscopy, Raman spectroscopy, Hall measurements, and density functional theory calculations. At the initial stages of the intercalation, dopants typically increase the disorder in graphite. Moreover, the disorder density decreases for increasing intercalation, implying quasi-structural ordering in the intercalated compound. Results reported here allow us to tune the Fermi level (work function) and the carrier density in the few-layer graphene and graphite. We believe that such results are especially interesting for modifying the physical properties of few-layer graphite grown onto SiC by thermal decomposition method where the individual layers behave as graphene sheets and grants future studies.

Acknowledgments

J. Li gratefully acknowledges financial support from the National Science Fund for Distinguished Young Scholar (Grant No. 60925016) and the National Natural Science Foundation of China (Grant No. 11104250). This work at UC Berkeley is supported by the U.S. Department of Energy Early Career Award DE-FG02-11ER46796.

REFERENCES

[1] Dresselhaus MS, Dresselhaus G. Intercalation compounds of graphite. Adv Phys 2002;51(1):1–186.
[2] Enoki T, Suzuki M, Endo M. Graphite intercalation compounds and applications. New York: Oxford; 2003. p. 1–8.
[3] Cheng HS, Sha XW, Chen L, Cooper AC, Foo ML, Lau GC, et al. An enhanced hydrogen adsorption enthalpy for fluoride intercalated graphite compounds. J Am Chem Soc 2009;131(49):17732–3.
[4] Tsang JC, Freitag M, Perebeinos V, Liu J, Avouris PH. Doping and phonon renormalization in carbon nanotubes. Nat Nanotechnol 2007;2(11):725–30.
[5] Grüneis A, Attaccalite C, Rubio A, Vyalikh DV, Molodtsov SL, Fink J, et al. Angle-resolved photoemission study of the graphite intercalation compound KC_8: a key to graphene. Phys Rev B 2009;80(7):075431–5.
[6] Pisana S, Lazzeri M, Casiraghi C, Novoselov KS, Geim AK, Ferrari AC, et al. Breakdown of the adiabatic Born–Oppenheimer approximation in graphene. Nat Mater 2007;6(3):198–201.
[7] Weller TE, Ellerby M, Saxena SS, Smith RP, Skipper NT. Superconductivity in the intercalated graphite compounds C_6Yb and C_6Ca. Nat Phys 2005;1(1):39–41.
[8] Hwang J, Carbotte JP, Tongay S, Hebard AF, Tanner DB. Ultrapure multilayer graphene in bromine-intercalated graphite. Phys Rev B 2011;84(4):041410–3.
[9] Tongay S, Hwang J, Tanner DB, Pal HK, Maslov D, Hebard AF. Supermetallic conductivity in bromine-intercalated graphite. Phys Rev B 2010;81(11):115428–33.
[10] Tongay S, Schumann T, Miao X, Appleton BR, Hebard AF. Tuning Schottky diodes at the many-layer-graphene/semiconductor interface by doping. Carbon 2011;49(6):2033–8.
[11] Crowther AC, Ghassaei A, Jung N, Brus LE. Strong charge-transfer doping of 1 to 10 layer graphene by NO_2. ACS Nano 2012;6(2):1865–75.

[12] Walter J, Boehm HP. Stability of graphite intercalation compounds with TaCl, or NbCl, against water or dilute acids—a study with XRD, SEM/EDS and electron microprobe analysis (EMPA). Carbon 1995;33(8):1121–7.
[13] Woodley SM, Catlow RA. Crystal structure prediction from first principles. Nat Mater 2008;7(12):937–46.
[14] Catlow RA, Bromley ST, Hamad S, Fonz MM, Sokola AA, Woodley SM. Modelling nano-clusters and nucleation. Phys Chem Chem Phys 2010;12(4):786–811.
[15] Deaven DM, Ho KM. Molecular geometry optimization with a genetic algorithm. Phys Rev Lett 1995;75(2):288–91.
[16] Fan HY, Lampinen JJ. A trigonometric mutation operation to differential evolution. Global Optim 2003;27(1):105–29.
[17] Liu DC, Nocedal J. On the limited memory method for large scale optimization. Math Program B 1989;45(3):503–28.
[18] Blöchl PE. Projector augmented-wave method. Phys Rev B 1994;50(24):17953–79.
[19] Kresse G, Joubert D. From ultrasoft pseudopotentials to the projector augmented-wave method. Phys Rev B 1999;59(3):1758–75.
[20] Kresse G, Hafner J. Ab initio molecular dynamics for liquid metals. Phys Rev B 1993;47(1):558–61.
[21] Kresse G, Furthmüller J. Efficient iterative schemes for ab initio total-energy calculations using a plane-wave basis set. Phys Rev B 1996;54(16):11169–86.
[22] Perdew JP, Burke K, Ernzerbof M. Generalized gradient approximation made simple. Phys Rev Lett 1996;77(18):3865–8.
[23] Monkhorst HJ, Pack JD. Special points for Brillouin-zone integrations. Phys Rev B 1976;13(12):5188–92.
[24] Lang HP, Wiesendanger R, Thommen-Geiser V, Güntherodt H-J. Atomic-resolution surface studies of binary and ternary alkali-metal–graphite intercalation compounds by scanning tunneling microscopy. Phys Rev B 1992;45(4): 1829–37.
[25] Inagaki M, Mittal J, Vignal V, Watanabe G, Konno H. Synthesis, structure and stability of $MoCl_5$–graphite intercalation compounds. Int J Inorg Mater 1999;1(1):39–45.
[26] Tersoff J, Hamann DR. Theory of the scanning tunneling microscope. Phys Rev B 1985;31(2):805–13.
[27] Guo DH, Kondo T, Machida T, Iwatake K, Okada S, Nakamura JJ. Observation of Landau levels in potassium-intercalated graphite under a zero magnetic field. Nat Commun 2012;3(1068):1–6.
[28] Zhao WJ, Tan PH, Liu J, Ferrari AC. Intercalation of few-layer graphite flakes with $FeCl_3$: Raman determination of Fermi level, layer decoupling and stability. J Am Chem Soc 2011;133(15):5941–5.
[29] Zhang Yan, Zhang Zhuxia, Li Tianbao, Liu Xuguang, Xu Bingshe. XPS and XRD study of $FeCl_3$–graphite intercalation compounds prepared by arc discharge in aqueous solution. Spectrochimi Acta [A] 2008;70(5):1060–4.
[30] Das A, Chakraborty B, Piscanec S, Pisana S, Sood AK, Ferrari AC. Phonon renormalization in doped bilayer graphene. Phys Rev B 2009;79(15):155417–23.
[31] Ferrari AC, Robertson J. Interpretation of Raman spectra of disordered and amporphous carbon. Phys Rev B 2000;61(20):14095–107.
[32] Piscanec S, Piscanec S, Lazzeri M, Mauri F, Ferrari AC, Robertson J. Kohn anomalies and electron–phonon interactions in graphite. Phys Rev Lett 2004;93(18):185503–6.
[33] Elias DC, Nair RR, Mohiuddin TM, Morozov SV, Blake P, Halsall MP, et al. Control of graphene's properties by reversible hydrogenation: evidence for graphane. Science 2009;323(5914):610–3.
[34] Tongay S, Berke K, Lemaitre M, Nasrollahi Z, Tanner DB, Hebard AF, et al. Stable hole doping of graphene for low electrical resistance and high optical transparency. Nanotechnology 2011;22(8):425701–6.
[35] Thomsen C, Reich S. Double resonant Raman scattering in graphite. Phys Rev Lett 2000;85(24):5214–7.
[36] Jorio A, Dresselhaus MS, Saito R, Dresselhaus G. Raman spectroscopy in graphene and related systems. Wiley; 2011.
[37] Ding J, Qiao Z, Feng W, Yao Y, Niu Q. Engineering quantum anomalous/valley Hall states in graphene via metal-atom adsorption: an ab initio study. Phys Rev B 2011;84(19):195444–53.
[38] Partoens B, Peeters FM. From graphene to graphite: electroni structure around the *K* point. Phys Rev B 2006;74(7):075404–14.